Myelination transition zone astrocytes are constitutively phagocytic and have synuclein dependent reactivity in glaucoma

Judy V. Nguyen[a], Ileana Soto[a], Keun-Young Kim[b], Eric A. Bushong[b], Ericka Oglesby[c], Francisco J. Valiente-Soriano[d], Zhiyong Yang[e], Chung-ha O. Davis[c], Joseph L. Bedont[a], Janice L. Son[c], John O. Wei[c], Vladimir L. Buchman[f], Donald J. Zack[e], Manuel Vidal-Sanz[d], Mark H. Ellisman[b], and Nicholas Marsh-Armstrong[a,c,e,1]

[a]The Solomon H. Snyder Department of Neuroscience, The Johns Hopkins University School of Medicine, Baltimore, MD 21205; [b]National Center for Microscopy and Imaging Research, Center for Research in Biological Systems, Department of Neurosciences, University of California at San Diego, La Jolla, CA 92093; [c]Hugo W. Moser Research Institute at Kennedy Krieger, Baltimore, MD 21205; [d]Department of Ophthalmology, Faculty of Medicine, Universidad de Murcia, 5-30003 Murcia, Spain; [e]Department of Ophthalmology, The Johns Hopkins University School of Medicine, Baltimore, MD 21205; and [f]School of Biosciences, Cardiff University, Cardiff CF10 3AX, United Kingdom

Edited* by Constance L. Cepko, Harvard Medical School/Howard Hughes Medical Institute, Boston, MA, and approved December 9, 2010 (received for review September 16, 2010)

Optic nerve head (ONH) astrocytes have been proposed to play both protective and deleterious roles in glaucoma. We now show that, within the postlaminar ONH myelination transition zone (MTZ), there are astrocytes that normally express Mac-2 (also known as Lgals3 or galectin-3), a gene typically expressed only in phagocytic cells. Surprisingly, even in healthy mice, MTZ and other ONH astrocytes constitutive internalize large axonal evulsions that contain whole organelles. In mouse glaucoma models, MTZ astrocytes further up-regulate Mac-2 expression. During glaucomatous degeneration, there are dystrophic processes in the retina and optic nerve, including the MTZ, which contain protease resistant γ-synuclein. The increased Mac-2 expression by MTZ astrocytes during glaucoma likely depends on this γ-synuclein, as mice lacking γ-synuclein fail to up-regulate Mac-2 at the MTZ after elevation of intraocular pressure. These results suggest the possibility that a newly discovered normal degradative pathway for axons might contribute to glaucomatous neurodegeneration.

DBA/2J mice | retinal ganglion cell | Sncg

Glaucoma, a neurodegenerative disorder that kills retinal ganglion cells (RGCs), affects more than 60 million people and is the second leading cause of blindness worldwide (1). In glaucomatous retinas, both astrocytes and Müller glia increase their reactivity (2, 3). Within the orbital portion of the optic nerve, astrocytes increase in number and reactivity (4). Within the optic nerve head (ONH), astrocytes also increase reactivity in glaucoma animal models and in the human disease (5). These ONH astrocytes are of particular interest as they enwrap axons at the location where damage would account for the arcuate vision field loss characteristic of glaucoma.

Here, we identify a spatially discrete population of astrocytes within the ONH, those at the myelination transition zone (MTZ), which express the phagocytosis-related gene Mac-2. Surprisingly, astrocytes throughout the ONH including the MTZ phagocytose large axonal evulsions even in unaffected mice. Mac-2 expression is increased in optic nerve astrocytes upon injury and at the MTZ in two mouse models of glaucoma. In glaucomatous mice, there are protease resistant forms of γ-synuclein, including at the MTZ. Further, mice lacking γ-synuclein fail to up-regulate Mac-2 at the MTZ in response to increased intraocular pressure (IOP). These results suggest the possibility that failure to properly clear axon-derived material at the MTZ, including γ-synuclein, may contribute to axon loss in glaucoma.

Results

Astrocytes at the MTZ Constitutively Express Mac-2, a Gene That Optic Nerve Astrocytes Up-Regulate upon Injury. We recently showed that, in DBA/2J mice, microglia within the orbital (myelinated) portion of the optic nerve up-regulate Mac-2 late in glaucomatous degeneration (4). Mac-2 is a gene implicated in phagocytosis of myelin by professional phagocytes such as microglia (6) and nonprofessional phagocytes such as Schwann cells (7). Now we find that Mac-2 is also expressed in a discrete band of cells at the ONH in unaffected mice, including young DBA/2J mice (Fig. 1*A*). The Mac-2 expression domain coincides with the position of the first oligodendrocytes, in a region hereafter referred to as the MTZ. Surprisingly, the cells that constitutively express Mac-2 are astrocytes, as determined by their expression of GFAP (Fig. S1*A*, control) and Aldh1l1 and vimentin (Vim) mRNAs (Fig. 1*B*), and their lack of expression of the microglial marker Iba1 (Fig. 1*B*). To determine whether Mac-2 might be a marker of increased reactivity in astrocytes, optic nerves were analyzed 3 d after crush of the orbital optic nerve near the MTZ. Such crush produced an increase in GFAP and a larger increase in Mac-2 immunoreactivity (Fig. S1*A*). Measuring the mean Mac-2 fluorescence in pixels selected by their GFAP expression demonstrated that most of the Mac-2 increase after crush occurs within astrocytes: mean Mac-2 expression was approximately twofold higher in the crushed optic nerves and increased at higher segmentation values of GFAP (Fig. S1*B*). Nerves subjected to all surgical manipulations other than the crush itself ($n = 4$) had no Mac-2 up-regulation. Thus, Mac-2 is up-regulated in optic nerve astrocytes after injury and there is a population of optic nerve astrocytes that constitutively express high levels of Mac-2 in the absence of an external injury, namely the MTZ astrocytes.

MTZ Astrocytes Increase Mac-2 Expression During Glaucomatous Degeneration. To determine whether Mac-2 expression at the MTZ was further increased during axonal degeneration in glaucoma, 10-mo-old DBA/2J mice were compared with 3-mo-old DBA/2J mice. As previously reported (8), mouse RGCs can be identified by their expression of the RGC-specific gene

Author contributions: N.M.-A. designed research; J.V.N., I.S., K.-Y.K., E.A.B., E.O., F.J.V.-S., Z.Y., C.-h.O.D., J.L.B., J.L.S., and J.O.W. performed research; J.V.N., I.S., K.-Y.K., E.A.B., V.L.B., D.J.Z., M.V.-S., M.H.E., and N.M.-A. analyzed data; and N.M.-A. wrote the paper.

Conflict of interest statement: N.M.-A. and I.S. have a pending patent application on the use of anti-Parkinson disease treatments in glaucoma.

*This Direct Submission article had a prearranged editor.

Freely available online through the PNAS open access option.

Data deposition: The EM data sets reported in this paper have been deposited in the ccdb.ucsd.edu database (accession no. P2078).

[1]To whom correspondence should be addressed. E-mail: marsh-armstrong@kennedykrieger.org.

This article contains supporting information online at www.pnas.org/lookup/suppl/doi:10.1073/pnas.1013965108/-/DCSupplemental.

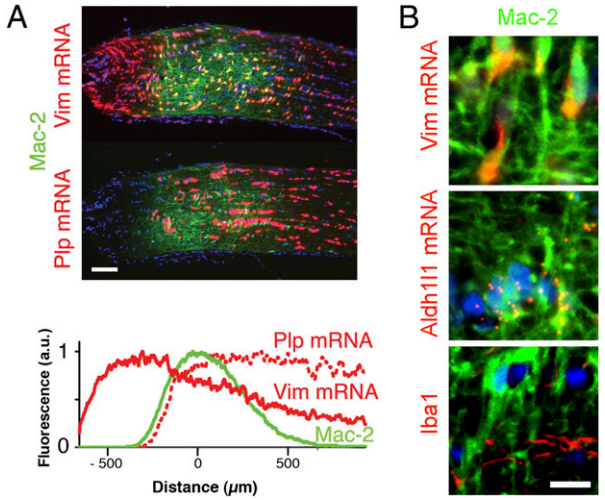

Fig. 1. A band of Mac-2–expressing astrocytes is located at the postlaminar optic nerve MTZ. (*A*) Mac-2–expressing cells form a band at the MTZ, as determined by the expression of the astrocyte-specific Vim mRNA and the oligodendrocyte-specific Plp mRNA. Histogram shows the expression of Vim mRNA (solid red), Plp mRNA (dotted red), and Mac-2 (green) as a function of distance from the center of Mac-2 expression. Values represent the mean of mean values from 10 nerves (an average of six sections per nerve). (*B*) Mac-2–expressing cells at the MTZ are astrocytes, based on the expression of astrocyte-specific Vim and Aldh1l1 mRNAs and lack of expression of the microglial marker Iba1. All images of the ONH in all figures are oriented with the eye to the left of the MTZ. (Scale bars: *A*, 100 μm; *B*, 10 μm.)

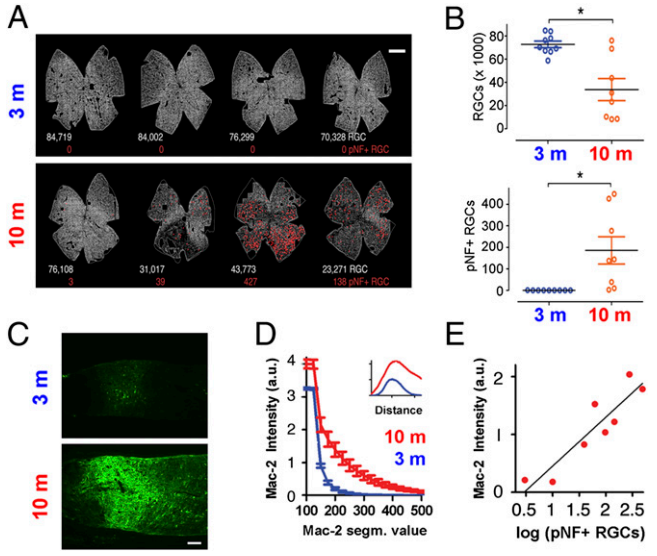

Fig. 2. Degenerating nerves in DBA/2J mice have a large increase in Mac-2 expression at the MTZ. (*A*) Retina whole mounts show RGCs, detected by γ-synuclein mRNA (gray), and the position of pNF+ RGCs (red dots). The number of RGCs and pNF+ RGCs are shown below each retina in white and red, respectively. (*B*) The number of RGCs was lower and the number of pNF+ RGCs higher in the 10-mo relative to the 3-mo DBA/2J mice. **P* = 0.003 (*Top*), **P* = 0.01 (*Bottom*), Mann–Whitney *t* test. (*C*) Mac-2 immunoreactivity at the MTZ in representative 3-mo and 10-mo DBA/2J mice. (*D*) Higher mean intensity of Mac-2 immunoreactivity at the MTZ in 10-mo relative to 3-mo DBA/2J at all segmentation values of Mac-2. For example, at a segmentation of 200, values were approximately sevenfold higher ($P < 0.001$, two-tailed unpaired *t* test). *Inset*: Expression of Mac-2 along the nerve axis, which peaks at the MTZ in nerves of both 3-mo and 10-mo DBA/2J mice. (*E*) Mac-2 intensity increases linearly for every log increase in the number of pNF+ RGCs (Pearson $r = 0.91$, $P < 0.001$). Values represent the mean of nine and eight eyes for the 3-mo and 10-mo mice, respectively. Error bars represent SEM. (Scale bars: *A*, 500 μm; *C*, 100 μm.)

γ-synuclein, and a subset of axonally damaged RGCs can be identified based on their having phosphorylated neurofilaments (pNFs) in their somas and dendrites (pNF^+ RGCs; Fig. S2). As expected, the 10-mo retinas had decreased numbers of RGCs, more than two orders of magnitude increase in the number of pNF^+ RGCs, and manifested sectorial patterns of degeneration (Fig. 2 *A* and *B*). In these same 10-mo DBA/2J mice, there was an approximately sevenfold increase in Mac-2 expression at the MTZ (Fig. 2 *C* and *D*). In the glaucomatous mice, the expression of Mac-2 spread beyond the MTZ into both the (unmyelinated) lamina region and within the (myelinated) orbital optic nerve, although it still peaked at the MTZ (Fig. 2*D*, *Inset*). To determine whether the level of Mac-2 expression at the MTZ was correlated with the amount of active RGC degeneration, Mac-2 expression was compared with the number of pNF^+ RGCs in the 10-mo DBA/2J samples. Indeed, the level of Mac-2 at the MTZ increased linearly for every order of magnitude increase in the number of pNF^+ RGCs (Fig. 2*E*). To rule out the possibility that Mac-2 up-regulation by MTZ astrocytes was caused by aging, a separate experiment compared 9- to 10-mo DBA/2J versus age-matched DBA/2J $Gpnmb^+$ mice (Fig. S3). As expected, there was a significant loss of RGCs and increased number of pNF^+ RGCs in DBA/2J compared with DBA/2J $Gpnmb^+$ mice (Fig. S3 *A* and *B*). Relative to the DBA/2J $Gpnmb^+$ mice, the DBA/2J mice had significantly higher Mac-2 expression at the MTZ at the levels of both protein and mRNA (Fig. S3 *C* and *D*).

Normal ONH Astrocytes Constitutively Internalize Evulsed Axonal Material. To determine whether astrocytes at the MTZ manifest a phagocytic phenotype similar to other Mac-2–expressing cells, an ONH from a control 9-m C57BL/6J mouse was analyzed by automated serial block-face scanning EM (*Methods*). Two large volumes were collected, one centered on the MTZ (1.6 million μm^3) and another covering a region from the glial lamina to the MTZ (1.2 million μm^3; Fig. 3*A*). [These datasets are available in the Cell Centered Database (9) as Project 2078, at cccb.ucsd.edu]. Both in the lamina (Fig. 3*B*) and the MTZ (Fig. 3*C*), axons were enwrapped by astrocytes with transverse orientation, as previously reported (10). Surprisingly, even in this strain, which does develop RGC loss with age (8), axons at the glial lamina (Fig. 3*D*) and MTZ (Fig. 3*E*) had numerous large accumulations of electron-dense granules immediately adjacent to astrocytic processes (protrusions) and other similar granule accumulations that were completely separated from axons and surrounded by astrocytes (evulsions). Serial sectioning confirmed that the evulsions were completely separated from the axons (Movies S1 and S2). Serial reconstruction of one such evulsion found it attached to the axon of origin by a thin stalk (Movie S3). Similar granule accumulations were also found fully within astrocytes at various stages of degradation (Fig. 3 *D* and *E*, *Right*; and Movies S4 and S5). To determine their frequency, granule accumulations were counted in subvolumes taken from the glial lamina and MTZ (136,000 μm^3 each; Fig. 3*A*). Fewer granule accumulations were found at the MTZ relative to the glial lamina (72 vs. 218 in equal volumes, not corrected for differing optic nerve diameters at the two locations). Although the mean radius of accumulations was comparable at the lamina (0.9 ± 0.2 μm) and MTZ (1.0 ± 0.4 μm), there was a larger variability at the MTZ because of the presence of several large accumulations. To determine whether ONH astrocytes had the molecular machinery necessary to internalize and process axonal debris, the expression of phagocytosis-related genes recently shown to be expressed in astrocytes (11) were examined. Indeed, many or all ONH astrocytes, including MTZ astrocytes, express several genes involved in the cell death engulfment defective pathway, in-

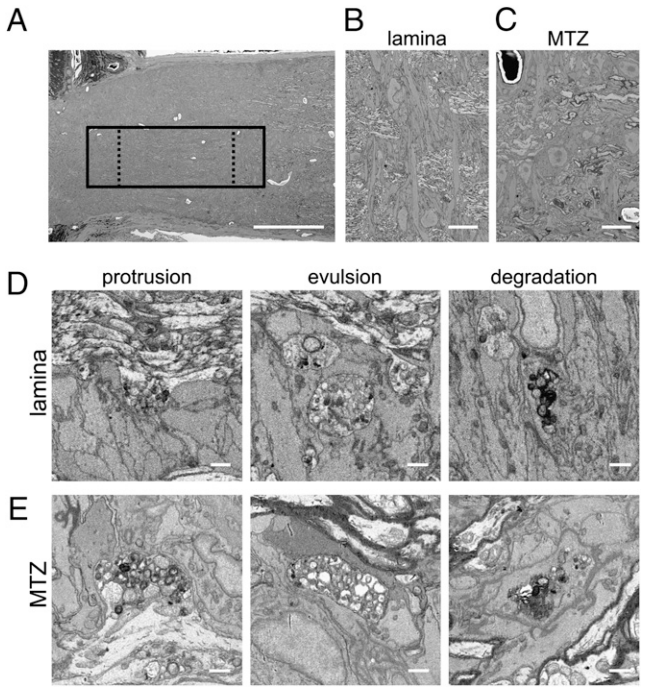

Fig. 3. ONH astrocytes internalize large axonal evulsions. (*A*) Low-power view of the ONH shows the location of one of two volumes acquired (solid box) and the regions used for counting granule accumulations in the lamina and MTZ (dashed boxes). (*B*) Low-power scanning EM view shows transverse astrocytes at the lamina. (*C*) Low-power scanning EM view of MTZ shows that astrocyte somata are also transversely oriented at the onset of myelination. In both the lamina (*D*) and the MTZ (*E*), granule accumulations exist as swellings and protrusions in axons (*Left*), as large evulsions completely separated from axons and completely ensheathed by astrocytes (*Center*), and as accumulations within the cytoplasm of astrocytes (*Right*). (Scale bars: *A*, 100 μm; *B* and *C*, 10 μm; *D* and *E*, 1 μm.)

cluding Abca1, Mfge8, Lrp1, and Pla2g7 (Fig. S4). Thus, like Mac-2–expressing microglia (6) and Schwann cells (7), Mac-2–expressing astrocytes at the MTZ are phagocytic.

MTZ Axonal Protrusions and Evulsions Contain γ-Synuclein. A previous study documented aberrant γ-synuclein accumulation in human glaucoma optic nerve, both in axonal spheroids and within astrocytes (12). To determine whether there was a relationship between the γ-synuclein pathologic processes observed in human glaucoma and the axonal protrusions/evulsions at the MTZ observed in DBA/2J mice, we used a custom antibody generated against the C-terminal 16 aa of mouse γ-synuclein. This antibody was deemed specific as it produced no labeling in sections of retina or optic nerve of $Sncg^{-/-}$ mice (Fig. S5 *A* and *B*). With the use of this antibody, γ-synuclein was found in axons colocalizing largely with neurofilaments in control mice, but was found inside cells in highly degenerated nerves of DBA/2J mice (Fig. S6 *A* and *B*). The γ-synuclein–positive cells were identified as astrocytes based on their expression of Vim mRNA (Fig. S6*B*), morphology, and enwrapping of blood vessels (Fig. S6*C*). Particularly in nerves with clear sectorial degeneration patterns (Fig. S6*D*), γ-synuclein also was found in large spheroidal structures. Thus, optic nerve pathologic processes involving γ-synuclein reported in human glaucoma (12) also occur in DBA/2J mice. Interestingly, in DBA/2J mice with sectorial degeneration patterns, these spheroids were largest and most numerous at the MTZ (Fig. S6*E*). Further, only some of the γ-synuclein–positive spheroids were contiguous with the axonal marker pNF (Fig. S6*F*), suggesting that some might not be connected to intact axons. In animals with no obvious RGC degeneration, smaller spheroidal structures resembling protrusions and evulsions labeled by γ-synuclein were evident at the MTZ, and were more frequent and larger in the older mice (Fig. S7*A*). Confocal analyses revealed that some of the γ-synuclein structures at the MTZ were fully inside Mac-2–expressing astrocytes (Fig. S7*B*). Thus, like the axonal spheroids and some astrocytes during glaucomatous degeneration, MTZ protrusions and evulsions contain γ-synuclein.

Some γ-Synuclein Becomes Protease Resistant During Glaucomatous Degeneration. To determine whether there might be protease-resistant forms of γ-synuclein in glaucoma similar to those observed for α-synuclein in Parkinson disease (13), both the antibody to the C terminus of γ-synuclein and a second γ-synuclein–specific antibody that does not label the C terminus of the protein (Fig. S5 *B–D*) were used to analyze retina sections from 3-mo and 10-mo DBA/2J mice. The loss of RGCs detected with the C terminus antibody (also see Fig. S2) coincided with increases in GFAP immunolabeling in astrocytes and Müller glia endfeet, and CD45 immunolabeling in microglia (Fig. 4*A*). The C terminus γ-synuclein antibody also labeled irregular structures within the inner plexiform layer (IPL) that were present only in the aged degenerating retinas. These irregular structures were labeled preferentially by the C terminus antibody (Fig. 4*B*, *Left*) and were

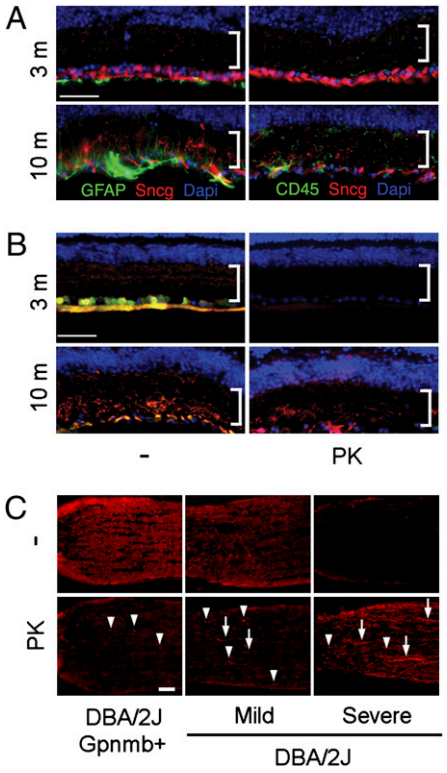

Fig. 4. Formation of PK-resistant γ-synuclein in glaucomatous retina and ONH. (*A*) Loss of γ-synuclein immunoreactivity (red) in aged DBA/2J coincides with increases in GFAP in glia and CD45 in microglia (green). Bracket shows the IPL. (*B*) Immunoreactivity of two γ-synuclein antibodies (red and green) is lost after PK treatment in healthy retinas of 3-mo DBA/2J mice, but much of the immunoreactivity of the C-terminal antibody (red) persists after PK treatment in degenerating retinas of 10-mo DBA/2J mice. (*C*) Protease-resistant γ-synuclein within the ONH during glaucomatous degeneration. Arrowheads point to examples of PK-resistant γ-synuclein in spheroids, and arrows point to examples of PK-resistant γ-synuclein in elongated processes. (Mac-2 expression in these same ONHs, and the RGCs and pNF+ RGCs in the corresponding retinas, are shown in Fig. S3). (Scale bars: 50 μm.)

resistant to digestion with proteinase-K (PK; Fig. 4*B*, *Right*). PK-resistant γ-synuclein was also found at the ONH (Fig. 4*C*). In control DBA/2J Gpnmb^{+} mice, only a few spheroidal structures at the MTZ contained PK-resistant γ-synuclein. In contrast, in degenerating DBA/2J mice, abundant PK-resistant γ-synuclein was found within both spheroids and processes resembling degenerating axons, even in nerves with very little γ-synuclein labeling visible in the absence of PK digestion (Fig. 4*C*, *Right*), suggesting that a significant fraction of γ-synuclein is detectable immunohistochemically only after PK digestion. Thus, there is formation of PK-resistant γ-synuclein in the retina and optic nerve during glaucomatous degeneration, including at the MTZ.

Mac-2 Up-Regulation at the MTZ After IOP Elevation Depends on γ-Synuclein. We next sought to determine whether γ-synuclein might play a role in the up-regulation of Mac-2 associated with axonal injury in glaucoma. To this end, Sncg$^{-/-}$ mice were compared with Sncg$^{+/-}$ mice 7 d after induced IOP elevation. The absence of γ-synuclein did not affect either the baseline IOP or the amount of IOP induced by translimbal laser photocoagulation (Fig. 5*A*) or the baseline amount of Mac-2 at the MTZ (Fig. 5*B*). However, unlike the heterozygous Sncg$^{+/-}$ mice, which had a significant increase in Mac-2 expression at the MTZ, the Sncg$^{-/-}$ mice failed to increase Mac-2 expression after IOP elevation (Fig. 5*B*). To determine whether γ-synuclein affected other IOP-dependent increases in glial reactivity, the expression of GFAP in the retina nerve fiber layer was analyzed. Translimbal lasering increased GFAP fluorescence on the retina surface, in astrocytes and Müller endfeet (Fig. S8*A*). Lasering produced a significant increase in GFAP, which unlike the expression of Mac-2 at the MTZ, was not significantly affected by γ-synuclein genotype (Fig. 5*C*). To determine if the lack of Mac-2 up-regulation at the MTZ was caused by a lack of retina damage in Sncg$^{-/-}$ mice, both the numbers of RGCs and pNF^{+} RGCs were examined. Neurofilament light (Nfl) mRNA was used to count RGCs as it labeled the same cells as γ-synuclein mRNA in retina whole mounts of C57BL/6J mice (Fig. S8 *B* and *C*). The current lasering protocol resulted in increased numbers of pNF^{+} RGCs but no large or sectorial loss of RGCs within 1 wk of IOP elevation (Fig. S8*D*). Overall RGC loss 1 wk after IOP elevation was small but significant ($P = 0.01$, two-way ANOVA, effect of lasering), although a more stringent statistical test showed it decreased only in Sncg$^{-/-}$ mice (Fig. 5*D*). Lasering produced increases of more than two orders of magnitude in the number of pNF^{+} RGCs, and Sncg$^{-/-}$ mice had approximately twice the number of pNF^{+} RGCs after lasering relative to Sncg$^{+/-}$ mice (Fig. 5*E*). Thus, the lack of Mac-2 up-regulation at the MTZ in Sncg$^{-/-}$ mice was not a result of less damage in the retina, as damage was even worse than in the mice that had γ-synuclein. Finally, Sncg genotype did not affect the amount of Mac-2 up-regulation by optic nerve astrocytes after optic nerve crush (Fig. 5*F*), showing that the effect of γ-synuclein is specific to glaucoma-like insults, to ONH astrocytes, or both. Altogether, these data demonstrate that γ-synuclein plays a significant and specific role in regulating Mac-2 expression by MTZ astrocytes after glaucomatous insults.

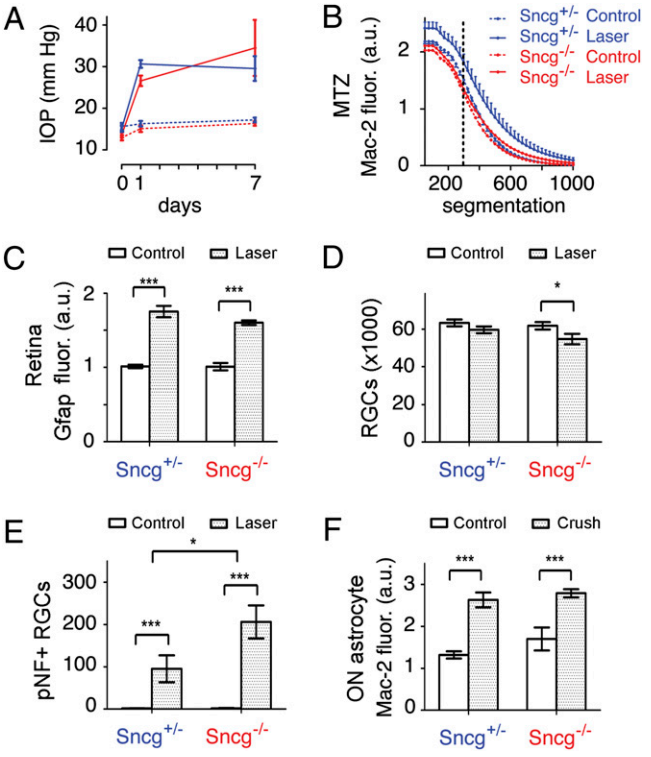

Fig. 5. IOP-dependent Mac-2 increase at the MTZ requires γ-synuclein. (*A*) γ-Synuclein does not affect the amount of IOP elevation produced by translimbal laser photocoagulation. (*B*) IOP elevation increases Mac-2 expression at the MTZ in mice with one copy of γ-synuclein (Sncg$^{+/-}$), but does not do so in mice that lack γ-synuclein (Sncg$^{-/-}$). For example, at the segmentation value of 300, marked by the dotted line, γ-synuclein genotype affects Mac-2 expression ($P = 0.01$, two-way ANOVA). SEM shown only for Sncg$^{+/-}$ mice for the sake of clarity, although SEM values were similar for Sncg$^{-/-}$ mice. (*C*) GFAP fluorescence on the retina surface is increased by lasering equally in Sncg$^{+/-}$ and Sncg$^{-/-}$ mice (***$P < 0.001$, two-way ANOVA). (*D*) Number of RGCs is decreased by lasering only in Sncg$^{-/-}$ mice (*$P < 0.05$, two-way ANOVA with Bonferroni posttest). (*E*) The number of pNF+ RGCs is increased by lasering in both Sncg$^{+/-}$ and Sncg$^{-/-}$ mice, but moreso in Sncg$^{-/-}$ mice. (*$P = 0.03$, two-way ANOVA effect of genotype; **$P < 0.05$ and ***$P < 0.001$, two-way ANOVA with Bonferroni posttest). (*F*) The Mac-2 fluorescence increase in optic nerve astrocytes (pixels selected by GFAP expression) observed 3 d after crush is not affected by Sncg genotype (***$P < 0.001$, two-way ANOVA with Bonferroni posttest). Values represent the mean of eight and six eyes for lasered eyes of Sncg$^{+/-}$ and Sncg$^{-/-}$ mice, five and six eyes for nonlasered control eyes in the lasering experiments, and six and seven eyes for Sncg$^{+/-}$ and Sncg$^{-/-}$ mice in optic nerve crush experiments. Error bars represent SEM.

Discussion

Possible Synucleinopathy in Glaucoma. Finding protease-resistant forms of γ-synuclein in glaucoma animal models is significant in light of the probable pathological role of protease resistant α-synuclein in Parkinson disease and related synucleinopathies (13). The idea that aggregated γ-synuclein might contribute to RGC loss is based on recent studies showing that overexpression of γ-synuclein results in an aging-dependent formation of dystrophic beaded neurites, spheroids, and inclusions within neurons, as well as astrogliosis (14). These pathological manifestations are similar to those observed in mice overexpressing α-synuclein and in patients with α-synucleinopathies (15, 16). We show here that protease-resistant γ-synuclein is found at two major sites of glaucoma pathology in DBA/2J mice, the IPL and the ONH. Finding protease-resistant γ-synuclein at the ONH and demonstrating that increased reactivity of a subset of ONH astrocytes depends on γ-synuclein is significant, as this is a location where damage to axons can give rise to the sectorial pattern of RGC loss that characterizes human glaucoma (17) and the loss of RGCs in the DBA/2J mouse (8, 18, 19) and some other rodent models of glaucoma (20, 21). Astrocytes and dystrophic axons containing γ- but not α- or β-synuclein have already been reported within the optic nerve in human glaucoma (12). Thus, based on the current and previous studies, aberrant forms of γ-synuclein are associated with pathological manifestations of glaucoma. However, much work is needed to determine whether γ-synuclein aggregates contribute to the loss of RGCs in glaucoma, or rather whether the observed γ-synuclein pathologic

processes merely represents a by-product of degeneration. We show here that, soon after sudden and large IOP elevation, mice that lack γ-synuclein fail to up-regulate Mac-2 and develop more axonal loss. These results suggest that, acutely after IOP increases, γ-synuclein plays a protective function for axons. Whether γ-synuclein can also play a pathological role in a low and chronic IOP age-dependent glaucoma, such as that seen in the DBA/2J mouse, remains to be determined.

ONH Astrocytes Are Constitutively Phagocytic. In the mammalian central nervous system, microglia are the major phagocytic cell, and together with macrophages are the principal means of clearing axonal debris during Wallerian degeneration (22). However, phagocytic activity by astrocytes has been reported in mammals after experimental trauma (23, 24), in response to glioma (25), and during developmental axonal death (26). Further, in non-mammalian vertebrates such as goldfish, astrocytes rather than microglia are principally responsible for clearing optic nerve debris during Wallerian degeneration (27). What is most surprising about the ONH astrocytes is not that they can phagocytose axons, but that they do so constitutively in the noninjured optic nerve and through large internalizations of axonal cytoplasm and organelles derived from intact axons. The cellular and molecular mechanisms deployed to accomplish such phagocytosis while preserving axonal integrity are not known, but may involve the same pathway used in axonal pruning during Drosophila metamorphosis (28), as we show here that ONH astrocytes express some of these same genes. The purpose of such bulk axonal phagocytosis at the ONH is also unknown. It may be a mechanism to degrade retrogradely transported materials too large to pass through the narrow lamina region without causing damage. Alternatively, it may be a homeostatic or stress-induced mechanism to degrade locally damaged organelles.

MTZ Astrocytes as Possible Mediators of Axonal Injury in Glaucoma. We have identified a subpopulation of ONH astrocytes based on their constitutive expression of Mac-2. As a gap has been described between laminar astrocytes and the beginning of myelination in the mouse optic nerve (29), these astrocytes should be categorized as a subset of postlaminar astrocytes. They are here named MTZ astrocytes because of their location. This location is unique in three important aspects. First, it is the position where astrocytes enwrap the first (hemi)node of Ranvier, a unique environment in terms of axonal transport and energy metabolism. Second, it is the position nearest to the vitreous where astrocytes contact pial septae filled with cerebrospinal fluid (30). This position may enable these astrocytes to sense the translaminar pressure differentials that have been recently implicated in glaucoma (31). Third, they are different from other ONH astrocytes in that they surround myelinated axons. Because the only gene identified so far that distinguishes MTZ astrocytes from other ONH astrocytes, Mac-2, is a marker associated with the degradation of myelin by professional (6) and non-professional (7) phagocytes, it is likely that both the normal and disease-related expression of Mac-2 by astrocytes at the MTZ is related to the phagocytosis of myelin that is uniquely required at this ONH location. Finding a previously unknown axon degradative pathway at the ONH of normal mice suggests a possible mechanism that might account for the sectorial nature of RGC loss in glaucoma. Failure by ONH astrocytes to clear axonal evulsions might lead to large focal accumulations of deleterious protein and lipid species capable of damaging whole axon fascicles. Determining whether such a mechanism contributes to axon loss in glaucoma is an important priority and should be the focus of further experimentation.

Methods

Animals. Experiments were carried out in accordance with the Association for Research in Vision and Ophthalmology statement for use of animals in research under protocols approved by the Animal Care and Use Committee at The Johns Hopkins University. C57BL/6J, DBA/2J, and DBA/2J Gpnmb^{+} (32) mice were obtained originally from Jackson Laboratories. The Sncg$^{-/-}$ mice (33), produced by V.L.B., were on a C57BL/6J background. All mice were bred and maintained at a pathogen-free facility at The Johns Hopkins University on a 12-h light/dark cycle with water and standard food provided ad libitum.

Translimbal Laser Photocoagulation and Optic Nerve Crush. IOP was elevated unilaterally using methods similar to those used in rats (34) as recently modified for mice (35), in 5- to 9-mo-old C57BL/6J Sncg$^{-/-}$ and Sncg$^{+/-}$ mice in groups matched for sex and age (7.6 and 7.5 mo, respectively). Burns were delivered directly behind the perilimbal plexus vessels (120–130 burns) and along the episcleral veins (15–20 burns) all around the limbus. IOP was measured with a rebound tonometer (TonoLab; Colonial Medical Supply). Only mice with peak pressures greater than 25 mm Hg were included in the study. Intraorbital crush to the optic nerve were delivered approximately 2 mm posterior to the globe for approximately 2 s using curved cross-action forceps (no. 7; Dumont), essentially as described (36).

Immunohistochemistry and in Situ Hybridization. γ-Synuclein immunohistochemistry used a custom antipeptide affinity-purified polyclonal antibody (Covance) or a commercial monoclonal antibody raised to recognize human γ-synuclein (Genetex). Protease-resistant γ-synuclein was detected by treating sections with 25 μg/mL PK for 5 min before incubation with the primary antibody. Other antibodies include those labeling GFAP (Sigma-Aldrich), CD45 (Abcam), Mac-2 (ATCC), pNF (SMI31; Covance), NFH (Chemicon), and Iba1 (Wako). RGC-5 cells were obtained from N. Agarwal (University of North Texas Health Science Center, Fort Worth, TX), and sequencing of the Thy1 gene confirmed that they were of mouse origin, as reported (37). Flat-mounted retinas were processed for in situ hybridization using digoxigenin- or fluorescein-labeled riboprobes for γ-synuclein and Nfl, transcribed from cDNAs (IMAGE clones 1448798 and 4506903; OpenBiosystems), hydrolyzed, and detected using Cy3 tyramides (Perkin-Elmer) for single in situ hybridizations, and both Alexa 488 (Invitrogen) and Cy3 tyramides for double in situ hybridizations, as previously described (8). RGC and pNF^{+} RGC numbers were estimated as previously described (8). In situ hybridization of longitudinal optic nerve cryostat sections, carried out as previously (4), used probes for Vim, Plp, Lgals3 (i.e., Mac-2), Abca1, Lrp1, Mfge8, and Pla2g7, generated from IMAGE clones 6517902, 5364736, 3257514, 524474, 385360, 3593310, and 3707891, respectively (OpenBiosystems). When practical, image quantification was carried out at varied segmentation values (selecting only pixels whose values were above a certain threshold), as others have done (38). All data were graphed and statistically analyzed by using GraphPad Prism (GraphPad Software).

Scanning Block-Face Serial EM. Scanning block-face serial EM employs a microtome inside of a scanning EM as originally described by Leighton (39) but recently refined by Denk and Horstmann (40). A labeling procedure (*SI Methods*) was developed for optimal resolution in scanning block-face serial EM based on lead aspartate labeling (41). Specimens were imaged on a Quanta SEM (FEI) equipped with a 3View serial block-face system (Gatan). Specimens imaged at high vacuum with 2.5-kV beam current and 70-nm sectioning thickness. A 2D montage was collected at each Z plane to increase field of view. Volumes were stitched and analyzed by using IMOD (http://bio3d.colorado.edu/imod/) (42).

ACKNOWLEDGMENTS. The authors thank Masako Terada for her assistance preparing 3View datasets for analysis. This work was supported principally by a Catalyst for a Cure Grant from the Melza M. and Frank Theodore Barr Foundation through the Glaucoma Research Foundation (to N.M.-A.). Additional support was received from National Eye Institute (NEI) postdoctoral fellowship Grant 5T32 EY07143-12 (to I.S.), Wellcome Trust Grant 075615/Z/04/z (to V.L.B.), Fundación Séneca Grant 04446/GERM/07 (to M.V.-S.), National Center for Research Resources Grant 5P41RR004050, the Human Brain Project DA016602 from NIDA and 5R01GM82949 from NIGMS (to M.H.E.), NEI Grants 5R01EY019305 and 5R21EY019737 (to D.J.Z.), the Guerrieri Family Foundation (D.J.Z.), and, for 3D EM, the International Retina Research Foundation and Lasker Foundation (M.H.E. and N.M.-A.).

1. Quigley HA, Broman AT (2006) The number of people with glaucoma worldwide in 2010 and 2020. *Br J Ophthalmol* 90:262–267.

2. Inman DM, Horner PJ (2007) Reactive nonproliferative gliosis predominates in a chronic mouse model of glaucoma. *Glia* 55:942–953.

3. WoldeMussie E, Ruiz G, Wijono M, Wheeler LA (2001) Neuroprotection of retinal ganglion cells by brimonidine in rats with laser-induced chronic ocular hypertension. *Invest Ophthalmol Vis Sci* 42:2849–2855.
4. Son JL, et al. (2010) Glaucomatous optic nerve injury involves early astrocyte reactivity and late oligodendrocyte loss. *Glia* 58:780–789.
5. Hernandez MR, Miao H, Lukas T (2008) Astrocytes in glaucomatous optic neuropathy. *Prog Brain Res* 173:353–373.
6. Rotshenker S (2009) The role of Galectin-3/MAC-2 in the activation of the innate-immune function of phagocytosis in microglia in injury and disease. *J Mol Neurosci* 39: 99–103.
7. Reichert F, Saada A, Rotshenker S (1994) Peripheral nerve injury induces Schwann cells to express two macrophage phenotypes: Phagocytosis and the galactose-specific lectin MAC-2. *J Neurosci* 14:3231–3245.
8. Soto I, et al. (2008) Retinal ganglion cells downregulate gene expression and lose their axons within the optic nerve head in a mouse glaucoma model. *J Neurosci* 28: 548–561.
9. Martone ME, et al. (2002) A cell centered database for electron tomographic data. *J Struct Biol* 138:145–155.
10. Sun D, Lye-Barthel M, Masland RH, Jakobs TC (2009) The morphology and spatial arrangement of astrocytes in the optic nerve head of the mouse. *J Comp Neurol* 516: 1–19.
11. Cahoy JD, et al. (2008) A transcriptome database for astrocytes, neurons, and oligodendrocytes: a new resource for understanding brain development and function. *J Neurosci* 28:264–278.
12. Surgucheva I, et al. (2002) Synucleins in glaucoma: Implication of gamma-synuclein in glaucomatous alterations in the optic nerve. *J Neurosci Res* 68:97–106.
13. Kahle PJ (2008) alpha-Synucleinopathy models and human neuropathology: Similarities and differences. *Acta Neuropathol* 115:87–95.
14. Ninkina N, et al. (2009) Gamma-synucleinopathy: Neurodegeneration associated with overexpression of the mouse protein. *Hum Mol Genet* 18:1779–1794.
15. Neumann M, et al. (2002) Misfolded proteinase K-resistant hyperphosphorylated alpha-synuclein in aged transgenic mice with locomotor deterioration and in human alpha-synucleinopathies. *J Clin Invest* 110:1429–1439.
16. van der Putten H, et al. (2000) Neuropathology in mice expressing human alpha-synuclein. *J Neurosci* 20:6021–6029.
17. Quigley HA, Addicks EM, Green WR (1982) Optic nerve damage in human glaucoma. III. Quantitative correlation of nerve fiber loss and visual field defect in glaucoma, ischemic neuropathy, papilledema, and toxic neuropathy. *Arch Ophthalmol* 100: 135–146.
18. Jakobs TC, Libby RT, Ben Y, John SW, Masland RH (2005) Retinal ganglion cell degeneration is topological but not cell type specific in DBA/2J mice. *J Cell Biol* 171: 313–325.
19. Schlamp CL, Li Y, Dietz JA, Janssen KT, Nickells RW (2006) Progressive ganglion cell loss and optic nerve degeneration in DBA/2J mice is variable and asymmetric. *BMC Neurosci* 7:66.
20. Salinas-Navarro M, et al. (2010) Ocular hypertension impairs optic nerve axonal transport leading to progressive retinal ganglion cell degeneration. *Exp Eye Res* 90: 168–183.
21. Soto I, et al. (2010) Retinal ganglion cell loss in a rat ocular hypertension model is sectorial and involves early optic nerve axon loss. *Invest Ophthalmol Vis Sci*, in press.
22. Vargas ME, Barres BA (2007) Why is Wallerian degeneration in the CNS so slow? *Annu Rev Neurosci* 30:153–179.
23. al-Ali SY, al-Hussain SM (1996) An ultrastructural study of the phagocytic activity of astrocytes in adult rat brain. *J Anat* 188:257–262.
24. Bechmann I, Nitsch R (1997) Astrocytes and microglial cells incorporate degenerating fibers following entorhinal lesion: a light, confocal, and electron microscopical study using a phagocytosis-dependent labeling technique. *Glia* 20:145–154.
25. Lantos PL (1974) An electron microscope study of reacting astrocytes in gliomas induced by n-ethyl-n-nitrosourea in rats. *Acta Neuropathol* 30:175–181.
26. Berbel P, Innocenti GM (1988) The development of the corpus callosum in cats: A light- and electron-microscopic study. *J Comp Neurol* 276:132–156.
27. Colavincenzo J, Levine RL (2000) Myelin debris clearance during Wallerian degeneration in the goldfish visual system. *J Neurosci Res* 59:47–62.
28. Logan MA, Freeman MR (2007) The scoop on the fly brain: Glial engulfment functions in Drosophila. *Neuron Glia Biol* 3:63–74.
29. Howell GR, et al. (2007) Axons of retinal ganglion cells are insulted in the optic nerve early in DBA/2J glaucoma. *J Cell Biol* 179:1523–1537.
30. Hogan MJ, Alvarado JA, Weddell JE (1971) *Histology of the Human Eye: An Atlas and Textbook* (Saunders, Philadelphia).
31. Ren R, et al. (2010) Cerebrospinal fluid pressure in glaucoma: A prospective study. *Ophthalmology* 117:259–266.
32. Howell GR, et al. (2007) Absence of glaucoma in DBA/2J mice homozygous for wild-type versions of Gpnmb and Tyrp1. *BMC Genet* 8:45.
33. Ninkina N, et al. (2003) Neurons expressing the highest levels of gamma-synuclein are unaffected by targeted inactivation of the gene. *Mol Cell Biol* 23:8233–8245.
34. Levkovitch-Verbin H, et al. (2002) Translimbal laser photocoagulation to the trabecular meshwork as a model of glaucoma in rats. *Invest Ophthalmol Vis Sci* 43: 402–410.
35. Salinas-Navarro M, et al. (2009) Functional and morphological effects of laser-induced ocular hypertension in retinas of adult albino Swiss mice. *Mol Vis* 15:2578–2598.
36. Li Y, Schlamp CL, Nickells RW (1999) Experimental induction of retinal ganglion cell death in adult mice. *Invest Ophthalmol Vis Sci* 40:1004–1008.
37. Van Bergen NJ, et al. (2009) Recharacterization of the RGC-5 retinal ganglion cell line. *Invest Ophthalmol Vis Sci* 50:4267–4272.
38. Stevens B, et al. (2007) The classical complement cascade mediates CNS synapse elimination. *Cell* 131:1164–1178.
39. Leighton SB (1981) SEM images of block faces, cut by a miniature microtome within the SEM - a technical note. *Scan Electron Microsc* Pt 2):73–76.
40. Denk W, Horstmann H (2004) Serial block-face scanning electron microscopy to reconstruct three-dimensional tissue nanostructure. *PLoS Biol* 2:e329.
41. Walton J (1979) Lead asparate, an en bloc contrast stain particularly useful for ultrastructural enzymology. *J Histochem Cytochem* 27:1337–1342.
42. Kremer JR, Mastronarde DN, McIntosh JR (1996) Computer visualization of three-dimensional image data using IMOD. *J Struct Biol* 116:71–76.